scientific reports

Check for updates

OPEN

Oxygen reservoir effect of Tungsten trioxide electrode on endurance performance of ferroelectric capacitors for FeRAM applications

Yejoo Choi[1,4], Jaemin Shin[2], Jinhong Min[3], Seungjun Moon[4], Daeyoung Chu[4,5], Donghwan Han[4,5] & Changhwan Shin[5]✉

The effect of W and WO_3 electrodes on the ferroelectric characteristics of HZO (Zr-doped HfO_2)-based MFM (metal-ferroelectric-metal) capacitors was investigated. During the deposition of tungsten, the W electrode was formed using only Ar gas, while the WO_3 electrode was formed using a mixture of Ar and O_2 gases. The W-based MFM capacitors exhibited superior remnant polarization ($2P_r$ of 107.9 μC/cm^2 at 700 °C) compared to the WO_3-based capacitors; however, their endurance performance was degraded. In contrast, the WO_3-based capacitors showed endurance performance enhanced by three orders of magnitude due to the oxygen-rich reservoir effect. The oxygen introduced during the deposition of WO_3 prevented the oxygen scavenging effect of tungsten. Consequently, excessive generation of oxygen vacancies in the HZO layer was suppressed, resulting in improved endurance performance. These results were quantitatively confirmed through TEM, XPS, and XRD analyses.

Hafnia-based ferroelectric random-access memory (FeRAM) has attracted tremendous interest as one of the future candidates for nonvolatile memory applications because of its thickness scalability and CMOS (complementary metal oxide semiconductor) process compatibility[1–7]. However, its endurance characteristic, which is one of the crucial reliability properties of FeRAM, is not comparable to that of commercialized memory devices like DRAM (Dynamic Random Access Memory). The endurance characteristics are significantly affected by interface traps, such as oxygen vacancies, in hafnia-based ferroelectric materials[8]. Therefore, optimizing the amount of oxygen vacancies in the ferroelectric layer is key to improving the endurance performance of ferroelectric-based devices. One of the crucial factors that governs the amount of oxygen vacancies in ferroelectric materials is the choice of material for the metal electrode. Tungsten has been widely used for ferroelectric devices because of its CMOS compatibility. Moreover, compared to TiN-based ferroelectric capacitors, ferroelectric capacitors with tungsten metal electrodes have shown better ferroelectricity due to their stronger tensile stress[9]. However, tungsten-based ferroelectric capacitors also exhibit poor endurance performance due to the strong oxygen scavenging effect of tungsten, which induces an excessive amount of oxygen vacancies in the ferroelectric layer[10].

In this work, the device performance of HZO-based metal-ferroelectric-metal (MFM) capacitors with two different metal electrodes (i.e., metallic tungsten for W-based capacitors and oxidized tungsten for WO_3-based capacitors) was compared and investigated for future FeRAM applications. O_2 gas was added during the deposition of the tungsten metal electrode to form an oxygen reservoir and to prevent the oxygen scavenging effect of the tungsten metal electrode. The ferroelectric characteristics, including the endurance performance of W- and WO_3-based MFM capacitors, were investigated. Quantitative analyses such as TEM, EDS, XPS, and GIXRD were conducted to analyze changes in the atomic bonding within the HZO layer and phase transitions in the W and WO_3 metal electrode layers.

Materials and methods

MFM (metal-ferroelectric-metal) capacitors were fabricated, as shown in Fig. 1 First, standard cleaning processes (i.e., SPM, SC-1, and SC-2) and diluted HF (1:50) cleaning were performed on (100) p-type Si wafers with a resistivity of < 0.005 Ω·cm. Then, the tungsten bottom electrode was deposited by DC sputtering. Note

[1]Department of Electrical and Computer Engineering, Sungkyunkwan University, Suwon 16419, Korea. [2]Department of Electrical Engineering, University of Notre Dame, Notre Dame, IN 46556, USA. [3]Department of Materials Science and Engineering, University of Michigan, Ann Arbor, MI 48109, USA. [4]Semiconductor R&D Center, Samsung Electronics, Hwaseong 18448, Republic of Korea. [5]School of Electrical Engineering, Korea University, Seoul 02841, Korea. ✉email: cshin@korea.ac.kr

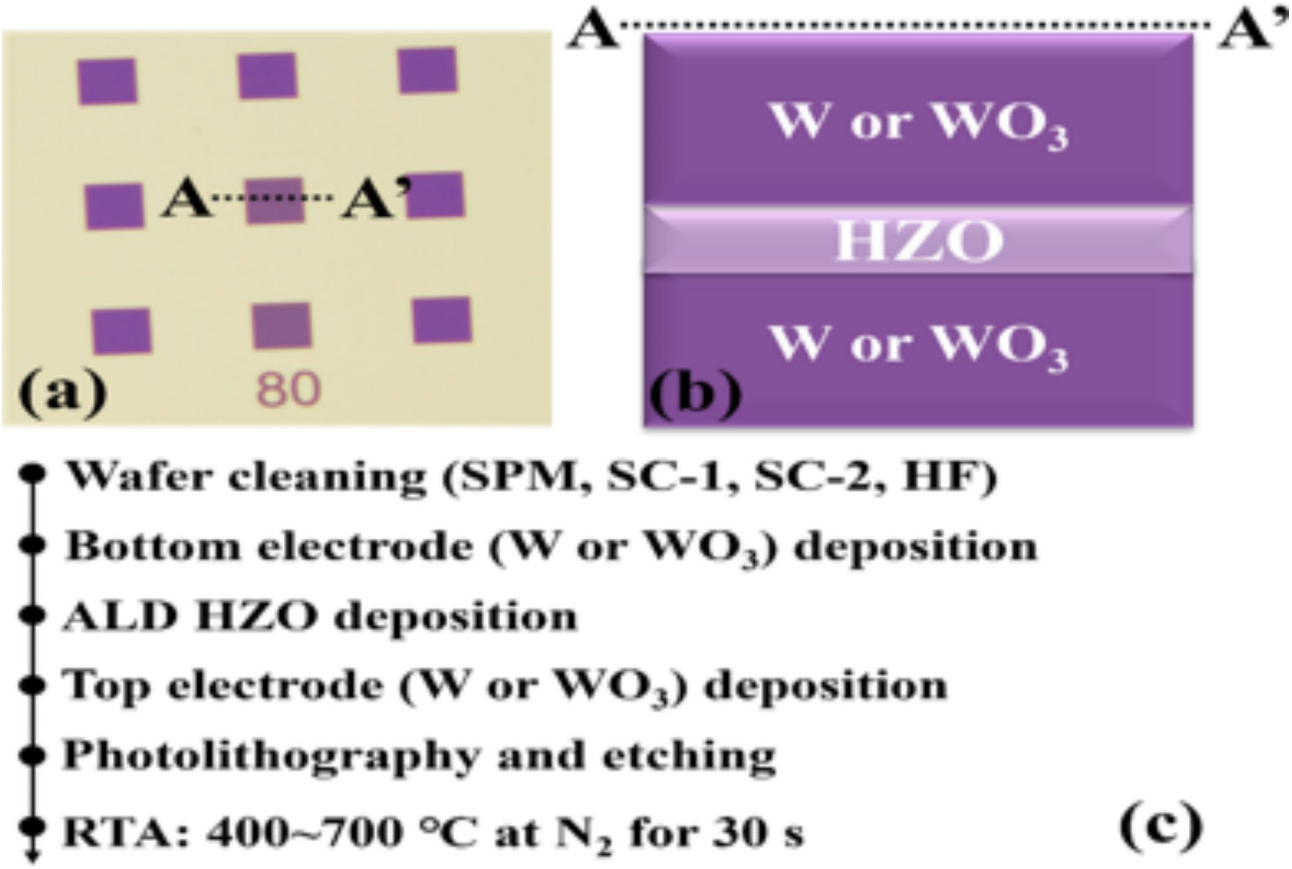

Fig. 1. (**a**) Microscopic image of ferroelectric capacitors with the area of 80 µm-by-80 µm. (**b**) Illustrated cross-sectional view and (**c**) fabrication process flow for the capacitor.

that two different gas flow conditions were used for the W deposition: (i) only Ar and (ii) Ar and O_2. The power and process time were identical for all samples. Afterwards, a 10-nm-thick HZO (Zr-doped HfO_2) layer was deposited by thermal ALD at a deposition temperature of 250 °C. Tetrakis (ethylmethylamino) hafnium (TEMAHf), tetrakis (ethylmethylamino) zirconium (TEMAZ), and H_2O were used as source precursors for the ALD process to deposit the HZO film. Subsequently, tungsten was deposited by DC sputtering for the top electrode, followed by photolithography, etching, PR ashing, and PR stripping to define the contact pattern. The device area size is 80×80 µm^2. The fabricated MFM capacitors were annealed at 400/500/600/700 °C for 30 s in an N_2 atmosphere using rapid thermal annealing (RTA) for post-metallization annealing (PMA) to crystallize the HZO film.

The device measurements were done with Keithley 4200 A-SCS parameter analyzer, to characterize the ferroelectric properties of those MFM capacitors. The current density versus voltage (I–V) and endurance characteristics were measured. A triangular waveform with the amplitude of 3 Vand 4 V was used to characterize the polarization-voltage (P-V) characteristics. A trapezoidal waveform with the amplitude of 3 V and 4 V was used for the endurance cycling. Note that the rise/fall time for both waveforms and the pulse width for trapezoidal waveform were set to 1 µs.

Results and discussions

Figure 2a and 2b show the Transmission Electron Microscopy (TEM) images and High Angle Annular Dark Field (HAADF) images from the Electron Dispersive Spectroscopy (EDS) of W- and WO_3-based capacitors at PMA temperature of 600 °C. As expected, W appeared in the top and bottom of the capacitor, while Hf and Zr were present in the intermediate layer. The EDS and XPS depth profiles in Fig. 2c and 2d confirmed that the oxygen content in the WO_3-based electrodes was significantly higher than that in W-based electrodes. The oxygen-rich nature of the WO_3 electrodes suggests a suppression of oxygen vacancies in the HZO layer, which is critical for improving endurance performance. The EDS analysis showed clear evidence of higher oxygen concentration in the top and bottom electrode layers of WO_3-based capacitors. This corroborates the hypothesis that WO_3 acts as an oxygen reservoir, preventing the oxygen scavenging effect of tungsten and thus reducing oxygen vacancy formation in the HZO layer. This is further supported by the XPS analysis in Fig. 3a and 3c, which showed a significant reduction in the oxygen vacancy-related suboxide peaks in WO_3-based capacitors.

XPS spectra of Hf 4f and W 4f were analyzed to further investigate the presence of oxygen vacancies. Figure 3a and c show the X-ray photoelectron spectroscopy (XPS) analysis of Hf 4f spectra from the HZO layer in W-

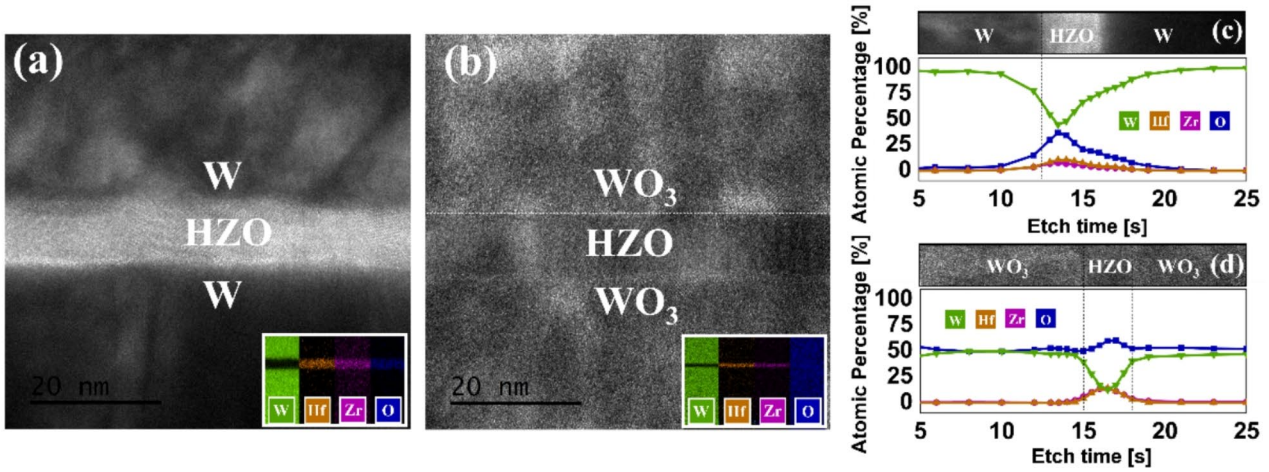

Fig. 2. TEM images and EDS analysis of (**a**) W-based MFM capacitor and (**b**) WO_3-based MFM capacitor. The XPS depth profile of (**c**) W-based MFM capacitor and (**d**) WO_3-based MFM capacitor.

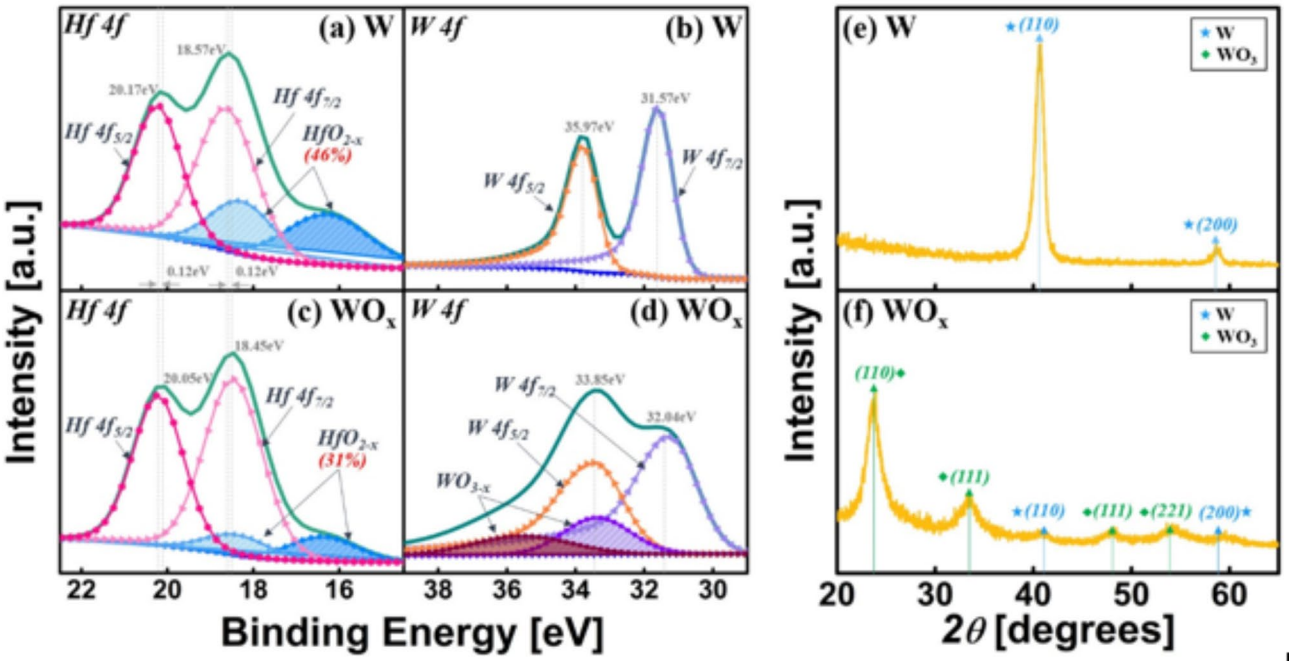

Fig. 3. XPS spectra of (**a**) Hf 4f and (**b**) W 4f in W-based capacitor. The XPS spectra of (**c**) Hf 4f and (**c**) W 4f in WO_3-based capacitor. GIXRD diffractogram for (**e**) W-based capacitor and (**f**) WO_3-based capacitor.

and WO_3-based capacitors at PMA temperature of 600 °C. For W-based capacitors in Fig. 3a, the Hf 4f peaks appeared at higher binding energies (18.57 and 20.17 eV), indicating a higher concentration of oxygen vacancies in the HZO layer. The suboxide peak (HfO_{2-x}) was prominent, making up approximately 46% of the total Hf 4f area, which signifies the existence of oxygen-deficient regions in the ferroelectric layer. The HfO_{2-x} peak in the figure represents the suboxide peak, which is oxygen-deficient HfO_{2-x}caused by the redox reaction, indicating the presence of oxygen vacancies in the HZO layer[11].

In contrast, the WO_3-based capacitors (Fig. 3c) exhibited lower binding energy peaks for Hf 4f (18.45 and 20.05 eV), with the suboxide peak contributing only 31% to the overall area. This reduction in oxygen vacancies can be attributed to the oxygen introduced during the deposition of WO_3, which helps fill the vacancies in the HZO layer. The XPS spectra of W 4f in Fig. 3b and d further confirmed this effect. While the W-based capacitors displayed strong peaks corresponding to metallic W (W $4f_{5/2}$ and W $4f_{7/2}$), the WO_3-based capacitors showed oxidized W states (WO_{3-x}), reflecting the oxygen-rich environment in these capacitors.

The added oxygen atoms can diffuse into the HZO layer and fill up the oxygen vacancies, as shown in Fig. 4. Tungsten metal exhibits a strong oxygen scavenging effect, inducing excessive oxygen vacancies and deteriorating the endurance performance, as observed in the W-based capacitor[12]. The addition of O_2 gas oxidizes the metallic tungsten to WO_3, creating an oxygen reservoir and suppressing the oxygen scavenging effect of W, as evidenced by the XPS analysis.

Figure 3e and 3f present the grazing-incidence X-ray diffraction (GIXRD) patterns in the range of 20 ~ 70° (2θ) for W- and WO_3-based capacitors. In the W-based capacitors, peaks corresponding to metallic W were observed around 40° and 60°. However, the WO_3-based capacitors exhibited additional peaks associated with tungsten oxides (WO_3), confirming the successful oxidation of the tungsten electrode. These results corroborate the XPS analysis of W 4f in Fig. 3b and 3d.

For various PMA temperatures, the measured pristine (before endurance cycling test) current density–vs.–voltage (I–V) and polarization–vs.–voltage (P–V) characteristics of W- and WO_3-based MFM capacitors are shown in Fig. 5. The P-V measurements were performed using a triangular pulse with an amplitude of 3–4 V. The endurance characteristics of each sample were measured, as shown in Fig. 6. A trapezoidal waveform with an amplitude of 3–4 V, a pulse width of 1 μs, and rising/falling times of 1 μs was used for the endurance cycling. The triangular pulse was used for the P-V measurements. Note that the endurance cycling pulse and P-V measurement pulse were set to the same value (i.e., 3 V/3V and 4 V/4V).

Table 1 summarizes the pristine $2P_r$ values and breakdown points in the endurance cycling of W- and WO_3-based capacitors at various PMA temperatures and pulse amplitudes. The W-based capacitors exhibited excellent $2P_r$ characteristics, with a maximum value of 107.9 μm/cm^2 at 700 ℃. The overall pristine $2P_r$ values of the WO_3-based capacitors were lower compared to the W-based capacitors. This reduction can be attributed to the excessive oxygen in WO_3, which causes the transformation of the o-phase to non-polar phases in the ferroelectric layer[12]. Although the pristine $2P_r$ of the WO_3-based capacitors was lower than that of the W-based capacitors, the endurance performance was significantly enhanced by up to 3 orders of magnitude. This improvement is due to the reduced oxygen vacancies resulting from the oxygen-rich WO_3electrode, as previously explained. Oxygen vacancies form undesirable conductive leakage paths in the HZO layer[13,14]. Consequently, the leakage paths were reduced with the decreased oxygen vacancies in the WO_3-based capacitors, leading to enhanced endurance performance.

As shown in Fig. 7a, the performance of the capacitors fabricated in this work was benchmarked against previous studies (which were annealed at various annealing temperatures). The MFM capacitors annealed at 400 to 700 ℃ showed superior $2P_r$ compared to the previous works. The unusually high $2P_r$ of 107.9 μC/cm² in the W/HZO/W capacitors is noteworthy. We attribute this high remnant polarization to the combined effects of tensile stress and enhanced crystallization at high annealing temperatures (up to 700 °C). The W electrodes induce significant tensile strain on the HZO layer, which promotes the stabilization of the orthorhombic ferroelectric phase, leading to higher polarization. In Fig. 7b, the number of maximum endurances cycling before the breakdown of each ferroelectric-based capacitor are summarized and compared to each other. It turned out that the MFM capacitors in this work (vs. previous works[8,10,15–22]) shows comparable endurance performance even with the superior $2P_r$ value showed in Fig. 7a. Although the pristine $2P_r$ of WO_3-based capacitors was lower than that of W-based capacitors, the superior endurance performance makes WO_3 a more viable candidate for FeRAM applications, where long-term reliability is critical. The trade-off between polarization and endurance performance highlights the importance of selecting electrode materials that can balance both properties effectively.

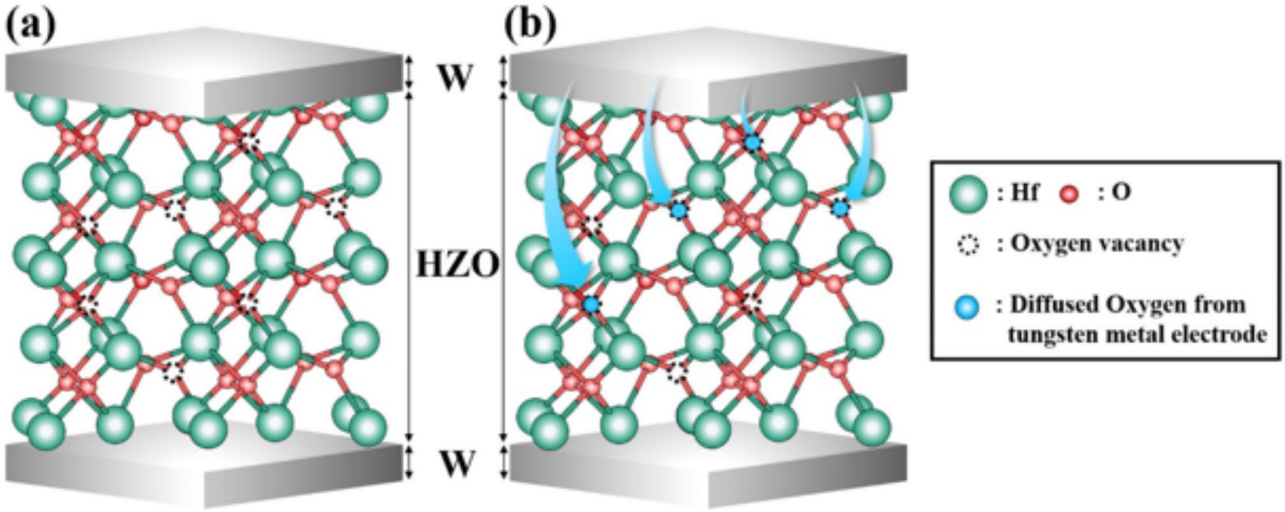

Fig. 4. Schematics of (**a**) atomic bonding of HfO_2 with oxygen vacancies in MFM capacitor. (**b**) Oxygen vacancies filled up with oxygen diffused from tungsten metal electrode.

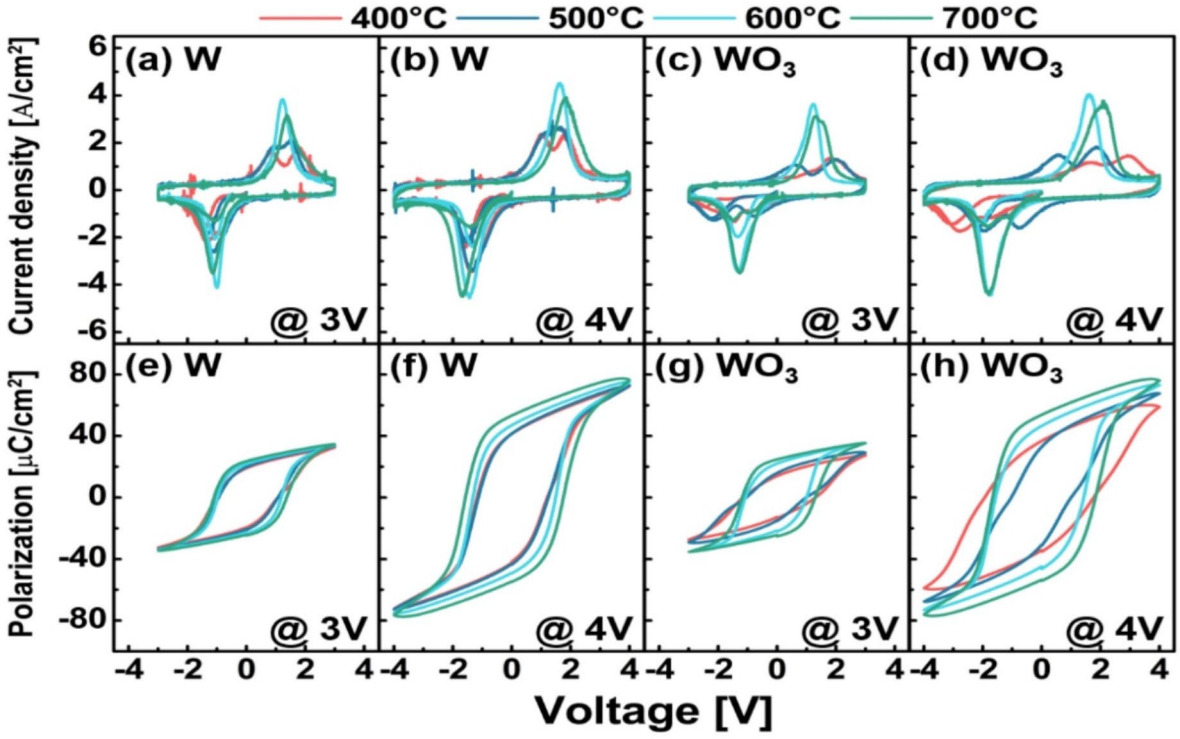

Fig. 5. (**a**-**d**) Measured "pristine" current density versus voltage, and (e-h) measured "pristine" polarization versus voltage for four different post metal annealing (PMA) temperatures at voltage amplitude of 3 and 4 V: (**a**), (**b**), (**e**), and (**f**) W-based capacitors. (**c**), (**d**), (**g**), and (**h**) WO_3-based capacitors.

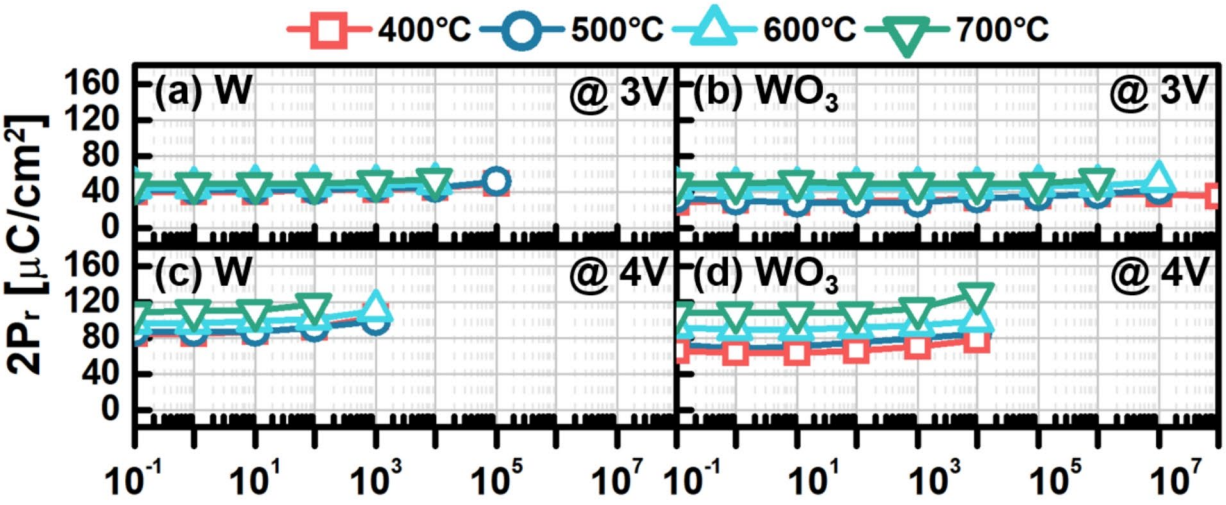

Fig. 6. Measured pristine $2P_r$ vs. the number of cycles of W-based MFM and WO_3-based MFM capacitors at (**a**, **b**) 3 V, (**c**, **d**) 4 V. The number of endurance cycle is 10^0~ 10^8. The 10^{-1} indicates the pristine state. The annealing temperature was set to four different annealing temperatures (i.e., 400, 500, 600, and 700 ℃).

Conclusion

The impact of W and WO_3 electrodes on HZO-based MFM capacitors was investigated and compared. The W-based MFM capacitors exhibited superior remnant polarization compared to the WO_3-based capacitors. However, the W-based capacitors showed deteriorated endurance performance. In contrast, the WO_3-based

Pristine $2P_r$ [$\mu C/cm^2$] / Breakdown point				
PMA Temp	@ 3V		@ 4V	
	W	WO_3	W	WO_3
400 °C	$38.4/10^5$	$26.7/10^8$	$83.9/10^3$	$65.9/10^4$
500 °C	$40.4/10^5$	$30.8/10^7$	$84.3/10^3$	$63.8/10^4$
600 °C	$44.5/10^4$	$43.5/10^7$	$96.1/10^3$	$91.5/10^4$
700 °C	$47.7/10^4$	$49.1/10^6$	$107.9/10^2$	$107.3/10^4$

Table 1. Pristine 2Pr and breakdown point of endurance cycling test.

capacitors demonstrated enhanced endurance performance due to the oxygen-rich reservoir effect. The added oxygen in WO_3 prevented the oxygen scavenging effect of tungsten, thereby suppressing the excessive generation of oxygen vacancies in the HZO layer, and consequently improving endurance performance. This result indicates that adjusting the Ar/O_2 gas ratio during the deposition of the tungsten metal can significantly affect the endurance performance of ferroelectric devices for future FeRAM applications.

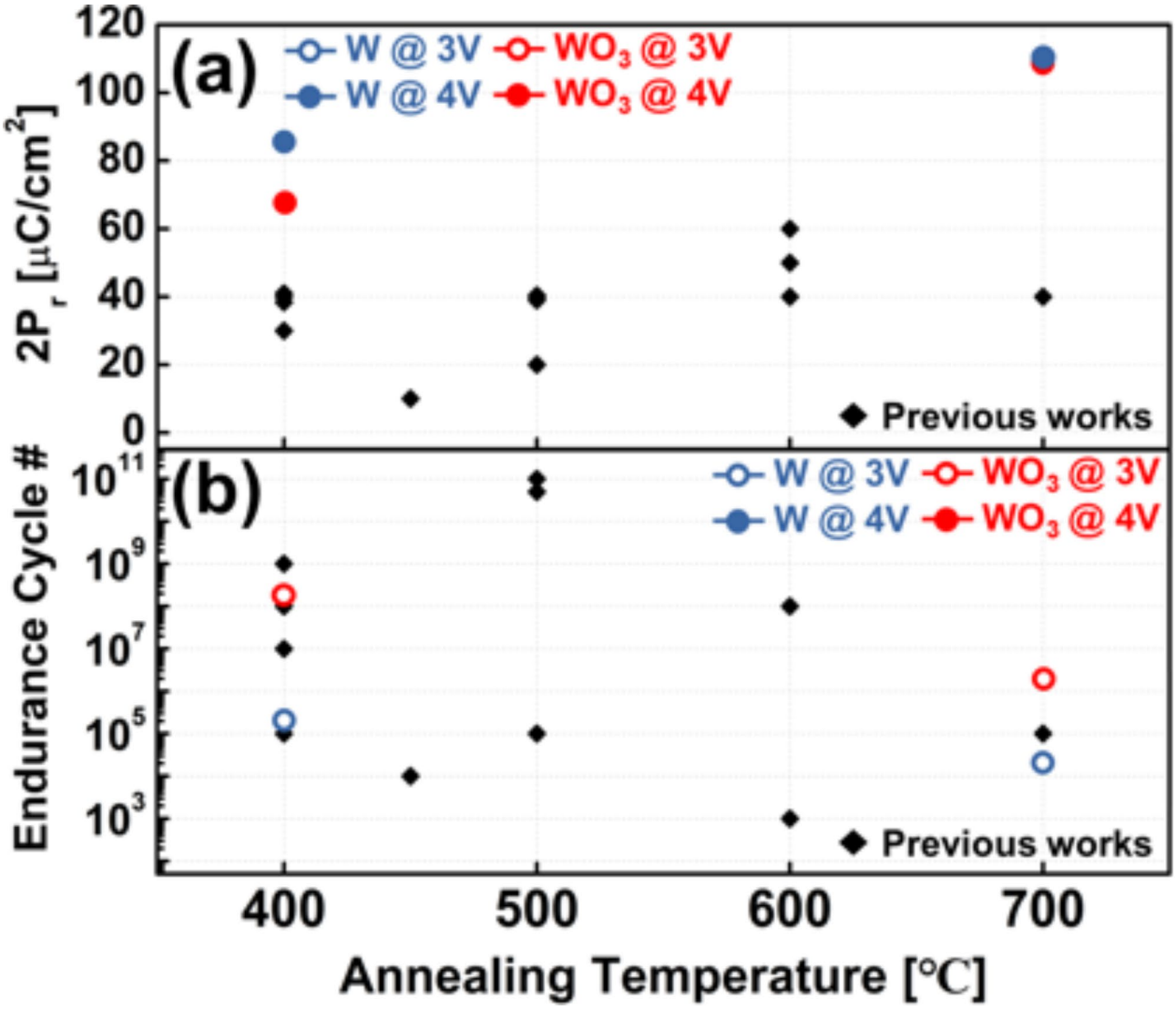

Fig. 7. The benchmarking plot of (**a**) $2P_r$ and (**b**) endurance characteristics of MFM capacitors in HfO_2-based ferroelectric capacitors with various annealing temperatures.

Data availability

The datasets generated during and/or analysed during the current study are available from the corresponding author on reasonable request.

Received: 18 August 2024; Accepted: 19 November 2024
Published online: 21 November 2024

References

1. Walke, A. M. et al. La Doped HZO based 3D-Trench Metal-Ferroelectric-Metal Capacitors with high endurance ($>10^{12}$) for FeRAM Applications. *IEEE Electron. Device Lett.* **45** https://doi.org/10.1109/LED.2024.3368225 (2024).
2. Grenouillet, L. et al. IEEE,. in 2020 *IEEE Silicon Nanoelectronics Workshop (SNW)* 5–6. (2020). https://doi.org/10.1109/SNW49134.2020.9109941
3. Okuno, J. et al. in. *IEEE International Memory Workshop (IMW)* 1–3. (2021). https://doi.org/10.1109/IMW51251.2021.9439392 (IEEE, 2021).
4. Choi, Y., Park, H., Han, C. & Shin, C. Impact of CF_4/O_2 plasma passivation on endurance performance of Zr-Doped HfO_2 ferroelectric Film. *IEEE Electron. Device Lett.* **44**, 713–716. https://doi.org/10.1109/LED.2023.3267221 (2023).
5. Lee, S. et al. Analysis of wake-up reversal behavior induced by imprint in La: HZO MFM capacitors. *IEEE Trans. Electron. Devices.* **70**, 2568–2574. https://doi.org/10.1109/TED.2023.3266815 (2023).
6. Choi, Y. et al. Experimental study of endurance characteristics of Al-doped HfO_2 ferroelectric capacitor. *Nanotechnology* **34**, 185203. https://doi.org/10.1088/1361-6528/acb1f3 (2023).
7. Min, J. et al. Program/erase scheme for suppressing interface trap generation in HfO_2-based ferroelectric field effect transistor. *IEEE Electron. Device Lett.* **42**, 1280–1283. https://doi.org/10.1109/LED.2021.3081966 (2021).

8. Mallick, A., Lenox, M. K., Beechem, T. E., Ihlefeld, J. F. & Shukla, N. Oxygen vacancy contributions to the electrical stress response and endurance of ferroelectric hafnium zirconium oxide thin films. *Appl. Phys. Lett.* 122. https://doi.org/10.1063/5.0133995 (2023).
9. Suh, Y. J. et al. Large polarization of $Hf_{0.5}$ $Zr_{0.5}O_x$ Ferroelectric Film on InGaAs with Electric-Field Cycling and Annealing Temperature Engineering. *IEEE Electron. Device Lett.* https://doi.org/10.1109/LED.2024.3369400 (2024).
10. Segantini, G. et al. Interplay between strain and defects at the interfaces of Ultra-thin $Hf_{0.5}Zr_{0.5}O_2$-Based Ferroelectric Capacitors. *Adv. Electron. Mater.* **9**, 2300171. https://doi.org/10.1002/aelm.202300171 (2023).
11. Lee, Y., Goh, Y., Hwang, J., Das, D. & Jeon, S. The influence of top and bottom metal electrodes on ferroelectricity of hafnia. *IEEE Trans. Electron. Devices*. **68**, 523–528. https://doi.org/10.1109/TED.2021.3049970 (2021).
12. Wang, X., Slesazeck, S., Mikolajick, T. & Grube, M. Modulation of Oxygen Content and Ferroelectricity in Sputtered Hafnia-Zirconia by Engineering of Tungsten Oxide bottom electrodes. *Adv. Electron. Mater.* **10**, 2300798. https://doi.org/10.1002/aelm.202300798 (2024).
13. Choi, Y. et al. Impact of chamber/annealing temperature on the endurance characteristic of Zr: HfO_2 ferroelectric capacitor. *Sensors* **22**, 4087. https://doi.org/10.3390/s22114087 (2022).
14. Park, M. H. et al. Effect of zr content on the wake-up effect in $Hf_{1-x}Zr_xO_2$ films. *ACS Appl. Mater. Interfaces*. **8**, 15466–15475. https://doi.org/10.1021/acsami.6b03780 (2016).
15. Lenox, M. K., Jaszewski, S. T., Fields, S. S., Shukla, N. & Ihlefeld, J. F. Impact of Electric Field Pulse Duration on Ferroelectric Hafnium Zirconium Oxide Thin Film Capacitor endurance. *Phys. Status Solidi A*. **221**, 2300566. https://doi.org/10.1002/pssa.202300566 (2024).
16. Cao, R. et al. Improvement of endurance in HZO-based ferroelectric capacitor using Ru electrode. *IEEE Electron. Device Lett.* **40**, 1744–1747. https://doi.org/10.1109/LED.2019.2937477 (2019).
17. Shao, X. et al. Investigation of endurance degradation mechanism of Si FeFET with HfZrO ferroelectric by an in situ V_{th} measurement. *IEEE Trans. Electron. Devices*. **70**, 3043–3050. https://doi.org/10.1109/TED.2023.3262482 (2023).
18. Lin, Y. D. et al. in. *IEEE International Electron Devices Meeting (IEDM)* 6.4.1–6.4.4. (2021). https://doi.org/10.1109/IEDM19573.2021.9720710 (IEEE, 2021).
19. Kim, S. J. et al. Low-thermal-budget (300°C) ferroelectric TiN/$Hf_{0.5}Zr_{0.5}O_2$/TiN capacitors realized using high-pressure annealing. *Appl. Phys. Lett.* **119** https://doi.org/10.1063/5.0058225 (2021).
20. Zhou, J. et al. Demonstration of ferroelectricity in Al-doped HfO_2 with a low thermal budget of 500°C. *IEEE Electron. Device Lett.* **41**, 1130–1133. https://doi.org/10.1109/LED.2020.3001798 (2020).
21. Chiniwar, S. P. et al. Ferroelectric enhancement in a TiN/$Hf_{1-x}Zr_xO_2$/W device with controlled oxidation of the bottom electrode. *ACS Appl. Electron. Mater.* **6**, 1078–1086. https://doi.org/10.1021/acsaelm.2c01434 (2024).
22. Lehninger, D. et al. Back-end-of-line compatible low-temperature furnace anneal for ferroelectric hafnium zirconium oxide formation. *Phys. Status Solidi A*. **217**, 1900840. https://doi.org/10.1002/pssa.201900840 (2020).

Acknowledgements

This study was supported by a National Research Foundation of Korea (NRF) grant (No. 2020R1A2C1009063 and RS-2023-00260527). Also, this work was supported by Samsung Electronics Co., Ltd (IO230412-05900-01).

Author contributions

Y.C. and C.S. conceived and designed all the experiments. Y.C. performed all the measurements. J.S., J.M., S.M., D.C., and D.H. participated in experimental works. Y.C., J.S., J.M., S.M., D.C., D.H., and C.S. discussed the results and wrote the manuscript.

Declarations

Competing interests

The authors declare no competing interests.

Additional information

Correspondence and requests for materials should be addressed to C.S.